

Modeling Entropic and Energetic Effects of Linker Length and Rigidity within Synthetic HIV-1 Antibodies designed to Bind Bivalently to Env Spikes

Tal Einav^a, Priyanthi N.P. Gnanapragasam^b, Shahrzad Yazdi^c, Rob Phillips^{a,b,d,*}, and Pamela J. Bjorkman^b

^aDepartment of Physics, California Institute of Technology, Pasadena, CA 91125

^bDivision of Biology and Biological Engineering, California Institute of Technology, Pasadena, CA 91125

^cDepartment of Materials Science and Engineering, Massachusetts Institute of Technology, Cambridge, MA, 02139, USA

^dDepartment of Applied Physics, California Institute of Technology, Pasadena, CA 91125

* Corresponding author

Abstract

Due to the low density of envelope (Env) spikes on the surface of HIV-1, neutralizing IgG antibodies rarely bind bivalently using both antigen-binding arms (Fabs) to crosslink between spikes (inter-spike crosslinking), instead resorting to weaker monovalent binding that is more sensitive to Env mutations. Antibodies capable of bivalently binding within single Env trimers (intra-spike crosslinking) should exhibit increased neutralization potencies. Here we consider synthetic diFabs joined by varying lengths of rigid double-stranded DNA (dsDNA). We asked whether linkers with different rigidities could enhance diFab potency by modeling DNA-Fabs containing different combinations of rigid dsDNA and flexible single-stranded DNA (ssDNA) and created a model that predicts their neutralization potencies. Model predictions showed that although a long flexible polymer may be capable of bivalent binding, it exhibits weak neutralization due to the large loss in entropic degrees of freedom during bivalent binding. In contrast, the strongest neutralization potencies were predicted to require a rigid linker that optimally spanned the distance between two Fab binding sites on an Env trimer. These results inform the design of bivalent anti-HIV-1 therapeutics that utilize avidity effects to remain potent against HIV-1 in the face of the rapid mutation of Env spikes.

Significance

Effective antibody-mediated immune responses against pathogens involve tight binding to invading particles. IgG antibodies usually accomplish this by simultaneously binding two antigen-binding arms (Fabs) to a dense array of antigens on the pathogen – if one Fab dissociates, IgGs can remain attached through the second arm, enhancing the likelihood that the first Fab will reassociate. This avidity effect enables bivalent IgGs to achieve a higher apparent affinity for the pathogen than a monovalent Fab. HIV-1 foils this strategy by having few, highly-separated, Envelope spikes (Envs) on its surface for IgGs to bind. This forces most anti-HIV-1 antibodies to bind monovalently, causing IgGs to rapidly dissociate from mutated strains of HIV-1 that arise during infection. In this work, we explore the predicted efficacies of an array of synthetic antibodies that achieve avidity through bivalent binding to single trimeric Envs. We develop a model that uses the geometry of each synthetic antibody to predict its neutralization potency, quantifying how entropic effects determine neutralization potencies and presenting a way to theoretically design an optimal antibody-based reagent that can bind bivalently to HIV-1 Env in order to target the virus in the face of its rapid mutation.

Introduction

Despite decades of research since its discovery, Human Immunodeficiency Virus-1 (HIV-1) continues to threaten global public health (1). While there have been advances in our understanding of the mechanisms of infection and the development of preventative and therapeutic strategies, there remains no cure for HIV-1 infection. Antiretroviral therapy with small molecule drugs can control the progression of the virus, allowing those infected with HIV-1 to live longer and healthier lives, but the treatment includes detrimental side effects, and when discontinued or not taken as prescribed, leads to viral rebound to pre-treatment levels (2). A major factor confounding the development of a prophylactic vaccine is the rapid mutation of HIV-1, leading to the emergence of many new strains, even within a single individual (3). Thus most antibodies raised by the host immune system are strain-specific or neutralize only a subset of strains, leading to viral escape from host antibodies.

Recent interest has focused upon the isolation of broadly neutralizing IgG antibodies (bNAbs) from a subset of HIV-1–infected individuals (4). These antibodies bind to and block the functions of the HIV-1 envelope (Env) spike, the viral protein responsible for fusion of the HIV-1 and target cell membranes that leads to entry of the virion's genetic material into the host cell (5). The discovery and characterization of HIV-1 bNAbs has brought new impetus to the idea of passively delivering antibodies to protect against or treat HIV-1 infection. bNAbs can prevent and treat infection in animal models (6-12) and exhibited efficacy against HIV-1 in human trials (13-16). However, HIV-1 Env mutates to become resistant to any single bNAb, as evidenced by the fact that NAb developed in an infected individual, even NAb that can neutralize large numbers of viral variants in laboratory assays, normally fail to neutralize autologous circulating viral strains (17-20). As a result, antibodies that develop during HIV-1 infection appear to be unable to control the virus in an infected individual.

We previously proposed that one mechanism by which HIV-1 evades antibodies more successfully than other viruses arises from the low surface density of Env spikes that can be targeted by neutralizing antibodies (21). Compared to viruses such as influenza A, dengue, and hepatitis B, the density of Env spikes on the surface of HIV-1 is about two orders of magnitude smaller (21). For example, influenza A has ≈ 450 spikes per virion, whereas each HIV-1 virion incorporates only 7-30 Env spikes (average of 14) (21-25), even though both are enveloped viruses with ≈ 120 nm diameters (Fig. 1A). The HIV-1 spikes are the machinery by which the virus binds its host receptor CD4 and coreceptor CCR5/CXCR4 to mediate the fusion of the host and viral membranes that allows its genome to enter target cells (5). As a consequence of its small number of spikes, HIV-1 infection of target cells is inefficient; the transmission probabilities for sexually-acquired HIV-1 infection range from 0.4 to 1.4% (26). However, the reduced infectivity of HIV-1 comes with a concomitant reduction in the ability of antibodies to control the virus, as the surface spikes serve as the only targets for neutralizing antibodies that can block infection of target cells (4).

The close spacing of spikes on typical viruses allows IgG antibodies to bind bivalently to neighboring spikes (inter-spike crosslinking) using both of their antigen-binding arms (Fabs). However, most spikes on HIV-1 virions are too far apart to permit inter-spike crosslinking by IgGs, whose antigen-binding sites are separated by ≤ 15 nm (27). While each homotrimeric HIV-1 spike includes three binding sites (epitopes) for an antibody, the architecture of HIV-1 Envs and distribution of epitopes on the HIV-1 Env trimer prohibits simultaneous binding of two Fabs within a single IgG (intra-spike crosslinking) to the same Env (28, 29). We suggested that predominantly monovalent binding by anti-HIV-1 antibodies expands the range of Env mutations

permitting antibody evasion, whereas reagents capable of bivalent binding through inter- or intra-spike crosslinking would be more resistant to Env mutations and thus more potent across multiple strains of HIV-1 (21). The hypothesis that HIV-1's low spike numbers and low densities contributes to the vulnerability of HIV-1 bNAbs to spike mutations is supported by independent biochemical and EM studies demonstrating that HIV-1 has an unusually low number of spikes that are not clustered (22-25, 30), and that bivalent IgG forms of anti-HIV-1 NAbs are only modestly more effective than monovalent Fabs, by contrast to bivalent IgGs against other viruses, which can be 100s- to 1000s-fold more potent than counterpart monovalent Fabs (21, 28, 29).

An antibody's neutralization potency against a virus is related to its antigen-binding affinity, which is defined as the binding strength between a Fab and its antigen (31) described by the equilibrium dissociation constant $K_D = \frac{[\text{Fab}][\text{Ag}]}{[\text{Fab-Ag}]}$, where [Fab], [Ag] and [Fab-Ag] are the concentrations of the antibody Fab, antigen, and the complex, respectively (32). In bivalent molecules interacting with binding partners that are tethered to a surface, the apparent affinity, or avidity, can be enhanced by multivalent binding. Such multivalent interactions are seen in many biological contexts including cell-cell communication, virus-host cell interactions, antibody-antigen interactions, and Fc receptor interactions with antigen-antibody complexes (33). Avidity effects benefit these interactions from both kinetic and thermodynamic standpoints: binding bivalently to tethered binding partners is advantageous kinetically because if one arm dissociates, the likelihood of it finding its binding partner is greater due to the constraint of being tethered (34). Avidity effects are also advantageous thermodynamically; whereas binding the first arm results in losses of translational and rotational degrees of freedom, the subsequent binding of the second arm incurs a smaller entropic cost, thereby increasing the likelihood of the bivalent state (34).

In the context of an IgG with two antigen-binding Fabs, the ability to bind bivalently is dependent on geometric factors such as the separation distances and orientations of tethered epitopes (35). In the case of IgG-virus interactions, the tethered epitopes would be on adjacent spikes during inter-spike crosslinking or on individual spikes if intra-spike crosslinking can occur. Although the architecture of the HIV-1 spike prevents intra-spike crosslinking (28, 29), it is possible to engineer reagents (homo- and hetero-diFabs) that can simultaneously bind to a single spike trimer. Our intra-spike crosslinking reagents were IgG Fabs joined by different lengths of double-stranded DNA (dsDNA), which served as both a rigid linker and a molecular ruler to probe the conformations of HIV-1 Env on virions (36) (Fig. 1B). Optimal diFabs should inhibit HIV-1 infection of reporter target cells more efficiently than the parental IgG or Fab. Since dsDNA behaves as a rigid rod for lengths up to 150 bps (37), the length of the dsDNA linker between the two Fabs could be used as a ruler to measure the approximate distance between epitope binding sites on virion Envs and to design reagents capable of strong intra-spike crosslinking between such sites.

While a rigid, optimal-length linker joining two HIV-1 bNAb Fabs should result in synergistic binding and neutralization of HIV-1 through avidity effects, we cannot rule out the possibility that a flexible linker joining two Fabs could also enhance potency. For example, if maximal potency in an intra-spike crosslinking diFab does not require a rigid linker spanning the precise distance between epitopes on trimeric HIV-1 Env, it should be possible to create IgGs that bind with avidity to any Env epitope using a protein-based flexible linker. A more flexible linker could potentially improve the antigen-binding orientation and hence affinity of the Fab, but it would also increase the entropic penalty associated with bivalent binding (34). To investigate which effect was dominant, flexible Gly₄Ser repeats were introduced into the hinge regions of IgGs to extend their reach, but the resulting constructs did not show increased potencies (38).

In this work, we modeled the predicted effects of 11 diFabs with DNA linkers to model the effects of linker rigidity on synergistic neutralization by a diFab constructed from the CD4-binding site bNAb 3BNC60. Starting with ($d=62$, $s=12$) (two 3BNC60 Fabs joined by a 62 bp (base pair) dsDNA linker flanked by 12 bases of ssDNA on both ends (36)), we considered new linker designs in order to predict the roles of rigidity and flexibility versus overall length of DNA linker within a series of 3BNC60 diFabs. We created a statistical mechanics-based mathematical model that characterized the various synthetic antibodies we created, which suggested that the efficacy of intra-spike crosslinking/increased neutralization potency could be explained solely by entropic effects. Using this model, we can predict the neutralization potential of other synthetic bivalent antibodies and of more complicated geometries involving additional Fabs. Insights from our synthetic constructs can be adapted to antibody design in other systems in which length and rigidity of linkers in multivalent reagents must be balanced to elicit the most effective response.

Results

Parameters for modeling

To evaluate our hypothesis that anti-HIV-1 reagents that bind bivalently would be more potent across multiple strains of HIV-1 (21), we previously engineered antibody-based molecules to bind bivalently through intra-spike crosslinking (36). This was accomplished by making a library of bNAb Fabs, covalently attached them to ssDNA, and then hybridizing the ssDNA to different lengths of dsDNA to make diFabs connected by different lengths of dsDNA (Fig. 1B). We hypothesized that the dsDNA in the bridging linker served as a molecular ruler by virtue of its long persistence length (dsDNA is essentially rigid up to ≈ 150 bp) and its 0.34 nm/bp increment (37). Optimal dsDNA linker length for the 3BNC60 diFab can be determined by evaluating dsDNA linkers using in vitro neutralization assays in which different concentrations of a synthetic antibody were evaluated for their ability to prevent HIV-1 infection of target cells (39). We previously found that the 50% inhibitory concentrations (IC_{50} values) of 3BNC60 diFabs were low (i.e., indicating potency) when the diFabs contained 62 bp of dsDNA with 12 bases of flanking ssDNA on both sides of the linker (36). We hypothesized that this diFab, here called ($d=62$, $s=12$), exhibited synergistic neutralization resulting from avidity effects due to intra-spike crosslinking in which the diFab bound to two of its three adjacent epitopes on a single HIV-1 Env trimer. The length of the double-stranded region of this linker (21 nm) was close to the predicted distance (≈ 20 nm) between the C-termini of adjacent 3BNC60 Fabs (where the DNA was covalently attached) bound to a low-resolution open structure of an HIV-1 trimer (40).

To model the linkers connecting the two Fabs in our synthetic antibodies, we treated the dsDNA as a 1D rigid rod and the ssDNA as a random walk. The former assumption is valid when the linkers in constructs include ≤ 100 bp of dsDNA, less than its 150 bp persistence length (41). Free ssDNA is flexible with a persistence length between 2-6 bases (42, 43), and because each of our the constructs we considered consisted of ssDNA segments with at least 12 bases, we analyzed the ssDNA as a floppy chain using polymer physics models (e.g., the ideal chain model, the worm-like chain model) (44).

The contribution of the ssDNA was modeled in two ways: (1) a model in which the ssDNA in the diFab linker was ignored by assuming it has zero length (Fig. 2A) and (2) a model in which the ssDNA contributed to the linker but with a smaller persistence length than when free in solution (Fig. 2B).

Another model parameter, l_{flex} , was included to account for variations in the distance between the C-termini of the two 3BNC60 C_H1 domains to which the DNA was attached due to the following factors: (i) The Fab C_H1-C_L domains can adopt different conformations with respect to V_H-V_L (45) such that the locations of the C_H1 C-terminus could shift by up to ≈ 1 nm, (ii) Residues C-terminal to C_H1 residue 217 are disordered in the 3BNC60 Fab structure (46), thus the position of the C_H1 residue to which the DNA was attached (Cys233) is uncertain within ≈ 1 nm, (iii) The ssDNA is covalently linked to the C_H1 residue Cys233 using an amine-to-sulfhydryl crosslinker (Sulfo-SMCC) (36), which would exert unknown effects on the length and the degree of flexibility between the ssDNA and Fab.

Relating Antibody Neutralization to the Probability that an HIV-1 Spike is Bound

We next created a mathematical model of diFab efficacy based on the properties of the linker. To lay the groundwork for this model, we first related the ability of a diFab to neutralize an HIV-1 virion to the probability that an Env spike on the surface of HIV-1 will be bound. Each Env spike is a homotrimer with three identical binding sites for a 3BNC60 Fab (47). The spikes are assumed to be sufficiently far apart that a diFab cannot crosslink between neighboring spikes. A diFab with the right geometry can bind to two binding sites on the same spike, whereas a diFab whose linker is either too short or too long can bind to only a single Env epitope.

Previous experiments suggested that only one of the three CD4 binding sites on an Env spike need to be bound to prevent the Env from functioning in membrane fusion (48). We imposed a soft threshold for virus entry where the ability of an HIV-1 virion to infect increases linearly from zero (when all spikes are bound by diFabs) to some maximum value (when all spikes are unbound) that is constant across all HIV-1 molecules (Appendix A). While some studies suggested that two or three Env trimers are required for HIV-1 to infect (49, 50), other studies found that only one functional Env trimer was required for target cell fusion (51); thus our model allowed a virion with a single unbound Env trimer to infect, albeit $1/n$ as effectively as a virion with n unbound trimers.

Given these assumptions, the ability of a diFab to neutralize HIV-1 is proportional to the probability that at least one of the CD4 binding sites of an HIV-1 spike will be bound by a 3BNC60 Fab (Appendix A). For example, if each Env protein has a 75% chance to be bound by a diFab, an average of 75% of the spikes on each virion will be bound, and by the linearity assumption, the HIV virions will be 75% neutralized. This enables us to relate the % neutralization for diFabs to the theoretically-tractable probability that a single Env spike will be bound either monovalently or divalently by a diFab. Avidity effects will allow an optimal diFab to bind more tightly (with a lower apparent K_D) to a spike, increasing the binding probability and the neutralization potency.

Modeling the Avidity of a diFab if it is Constrained by the Length of Rigid dsDNA and Essentially Independent of Flanking Flexible ssDNA

To calculate the probability that any of the 3BNC60 binding sites on an HIV-1 spike are occupied, we enumerated three potential states of the spike, which represent a single diFab bound to zero, one, or two adjacent binding sites. We first modeled the system as a pair of Fabs joined together with dsDNA and ignored the contributions of the ssDNA (Fig. 2A).

When a diFab transitions from the unbound state (with probability p_0) to a monovalently-bound state (with probability p_1), it loses translational and rotational entropy but gains favorable binding energy (52) leading to the relative probability

$$\frac{p_1}{p_0} = \frac{[Ab]}{K_D^{(1)}}, \text{ \# [Error! Bookmark not defined.]}$$

where $K_D^{(1)}$ is the equilibrium dissociation constant of the first diFab arm binding to Env. Note that $K_D^{(1)}$ incorporates the geometry of the Env trimer, namely, that there are three 3BNC60 binding sites on a trimeric HIV-1 spike and that the diFab can bind monovalently with either arm. Importantly, the transition from an unbound to a monovalently-bound diFab is independent of the composition of the diFab's linker, since the loss in translational and rotational entropy increases slowly with the size of a particle and hence can be assumed to be the same for all constructs. This implies that the constant $K_D^{(1)}$ will be the same for all diFabs and that it also characterizes the 3BNC60 Fab's binding to the Env trimer. By assuming that the neutralization potency of the Fab is proportional to how well it binds to the HIV-1 spike, the value of $K_D^{(1)}$ is given by an experimentally-determined Fab IC_{50} value for the 3BNC60 Fab against the 6535.3 strain of HIV-1 (74 ± 31 nM) (Fig. 3B), a value consistent with experimental K_D values reported for binding of a Fab from a CD4-binding site bNAb to a soluble, trimeric form of HIV-1 Env derived from a different HIV-1 strain (53). In viral contexts in which the relationship between the apparent K_D of an antibody and its IC_{50} is more complex, the dissociation constant could instead be inferred by nonlinear fitting.

We now turn to the transition from a monovalently-bound diFab to a bivalently-bound diFab. The ability to bivalently bind strongly depends on the size of the diFab's linker, since having too large or too small a linker will preclude bivalent binding through intra-spike crosslinking. The relative probability of each energy state is proportional to its Boltzmann weight, $e^{-\beta(E-TS)} = \Omega e^{-\beta E}$, where $\beta = \frac{1}{k_B T}$, E is the energy, T is the temperature (37°C), k_B represents Boltzmann's constant, $S = k_B \log \Omega$ is the entropy, and Ω is the number of microstates with a given energy. Thus, the relative probabilities of the bivalent and monovalent states satisfy

$$\frac{p_2}{p_1} = \frac{\Omega_2}{\Omega_1} e^{-\beta(E_2-E_1)} \text{ \# [Error! Bookmark not defined.]}$$

where p_j , E_j , and Ω_j represent the probability, energy, number of microstates when j Fabs are bound to an Env.

The number of configurations Ω_1 for a monovalently-bound diFab is proportional to the degrees of freedom available when one Fab is bound to its epitope and the second Fab is unbound and tethered to the first by DNA. Since the associated entropy of this motion increases slowly with size, we assume that Ω_1 is constant across all diFabs. Similarly, the binding energy $E_2 - E_1$ gained when the second Fab in a diFab binds to the HIV-1 spike is the same for all diFabs we consider.

The number of configurations Ω_2 of the bivalent state depend upon the entropy of the dsDNA linker joining the C-termini of the two bound Fabs separated by a width l_{linker} (Fig. 2A). In addition, each Fab is inherently flexible at the join between the C_H1 - C_L domains and the V_H - V_L domains, as denoted by l_{flex} . If we approximate l_{linker} and l_{flex} as colinear so that the problem becomes one dimensional (see Appendix B), the number of microstates corresponding to the bivalently-bound state satisfies

$$\Omega_2 = \frac{\max(l_{\text{flex}} - |l_{\text{dsDNA}} - l_{\text{linker}}|, 0)}{\Delta l} \equiv \frac{n(l_{\text{dsDNA}})}{\Delta l} \text{ \# [Error! Bookmark not defined.]}$$

where $n(l_{\text{dsDNA}})$ equals the length between the outer-most dsDNA orientations capable of bivalent binding (Appendix B Fig. S2), and Δl is a constant representing the discretization of this length so that Ω_2 is unitless. In short, $n(l_{\text{dsDNA}})$ quantifies how the geometry of the diFab affects its ability to bivalently bind to a spike.

Using Eqs. Error! Bookmark not defined.-Error! Bookmark not defined. and the normalization condition, $p_0 + p_1 + p_2 = 1$, the probability that at least one of the three Fab epitopes on an HIV-1 spike will be bound can be written as

$$p_1 + p_2 = \frac{\frac{[\text{Ab}]}{K_D^{(1)}} + \frac{[\text{Ab}]}{K_D^{(1)}} \alpha n(l_{\text{dsDNA}})}{1 + \frac{[\text{Ab}]}{K_D^{(1)}} + \frac{[\text{Ab}]}{K_D^{(1)}} \alpha n(l_{\text{dsDNA}})}} \#[\text{Error! Bookmark not defined.}]$$

where we have separated the constant $\alpha = \frac{1}{\Omega_1 \Delta l} e^{-\beta(E_2 - E_1)}$, which does not depend on the diFab geometry, from $n(l_{\text{dsDNA}})$, which does. Because $p_1 + p_2$ is proportional to the % neutralization of the HIV virion, the $\text{IC}_{50}^{\text{exc ssDNA}}$ of each diFab with the contribution of the ssDNA excluded is given by

$$\text{IC}_{50}^{\text{exc ssDNA}} = \frac{K_D^{(1)}}{1 + \alpha n(l_{\text{dsDNA}})} \#[\text{Error! Bookmark not defined.}]$$

We proceed by assuming that the dissociation constant takes the value $K_D^{(1)} = 74$ nM, which characterizes the first diFab arm binding to Env. We further assume an optimal linker length $l_{\text{linker}} = 21$ nm between bound Fabs, the flexibility $l_{\text{flex}} = 1.8$ nm between the Fab C_{H1}-C_L and V_H-V_L domains, and the avidity constant $\alpha = 70$. Fig. 2D (gray line) shows the model predictions, which roughly approximate the shape of the IC_{50} values. diFabs that are too long or too short cannot bivalently bind, leading to a sharp transition in the IC_{50} for dsDNA shorter than $l_{\text{linker}} - l_{\text{flex}} = 19.2$ nm (57 bp) or longer than $l_{\text{linker}} + l_{\text{flex}} = 22.8$ nm (69 bp). We hypothesized that including the ssDNA in the model would smooth the transition from the bivalent to purely monovalent binding, and next explored how the effects of the ssDNA in the linker could be modeled.

With contributions of ssDNA included, the distance l_{linker} between the C-termini of bivalently bound Fabs must be spanned by the rigid dsDNA segments as well as the two flanking ssDNA strands (Fig. 2B). We modeled each ssDNA segment as a random walk using an ideal chain model with a persistence length of $\xi_{\text{ssDNA}} = 0.1$ nm.

Of the multiple configurations that two ssDNA random walks can take on, only a small fraction will end at the proper distance l_{linker} to allow a diFab to bivalently bind. The probability density that the linker will obtain one of these limited configurations can be computed analytically (Appendix C) as

$$p(l_{\text{dsDNA}}, l_{\text{ssDNA}}, l_{\text{linker}}) = \frac{1}{l_{\text{linker}} l_{\text{dsDNA}}} \sqrt{\frac{3}{32\pi^3 l_{\text{ssDNA}} \xi_{\text{ssDNA}}}} e^{-\frac{3(l_{\text{linker}}^2 + l_{\text{dsDNA}}^2)}{8 l_{\text{ssDNA}} \xi_{\text{ssDNA}}}} \sinh\left(\frac{3 l_{\text{linker}} l_{\text{dsDNA}}}{4 l_{\text{ssDNA}} \xi_{\text{ssDNA}}}\right) \#[\text{Error! B}$$

where $l_{\text{dsDNA}} = d \left(0.34 \frac{\text{nm}}{\text{bp}}\right)$ and $l_{\text{ssDNA}} = s \left(0.64 \frac{\text{nm}}{\text{base}}\right)$ represent the length of dsDNA and ssDNA segments in the linker, respectively. Analogously to Eq. 3, the flexibility of the Fab implies that the dsDNA and ssDNA can span any length from $l_{\text{linker}} - l_{\text{flex}}$ to $l_{\text{linker}} + l_{\text{flex}}$ (see Appendix C).

In the limit where $1 \text{ nm} \approx l_{\text{flex}} \ll l_{\text{linker}} \approx 20 \text{ nm}$, the number of bivalent configurations is proportional to the simple form

$$\tilde{n}(l_{\text{dsDNA}}, l_{\text{ssDNA}}) = l_{\text{flex}}^2 p(l_{\text{dsDNA}}, l_{\text{ssDNA}}, l_{\text{linker}}). \quad \#[\text{Error! Bookmark not defined.}]$$

As in the model neglecting ssDNA described in the previous section, all other constants that are independent of the diFab geometry can be absorbed into a prefactor $\tilde{\alpha}$ in the bivalent state (Fig. 2B). Thus, the occupancy probability for an HIV-1 spike is given by the same functional form as Eq. Error! Bookmark not defined., namely,

$$p_1 + p_2 = \frac{\frac{[\text{Ab}]}{K_D^{(1)}} + \frac{[\text{Ab}]}{K_D^{(1)}} \tilde{\alpha} \tilde{n}(l_{\text{dsDNA}}, l_{\text{ssDNA}})}{1 + \frac{[\text{Ab}]}{K_D^{(1)}} + \frac{[\text{Ab}]}{K_D^{(1)}} \tilde{\alpha} \tilde{n}(l_{\text{dsDNA}}, l_{\text{ssDNA}})}} \quad \#[\text{Error! Bookmark not defined.}]$$

with an analogous IC_{50} given by

$$\text{IC}_{50}^{\text{inc ssDNA}} = \frac{K_D^{(1)}}{1 + \tilde{\alpha} \tilde{n}(l_{\text{dsDNA}}, l_{\text{ssDNA}})}. \quad \#[\text{Error! Bookmark not defined.}]$$

We proceed with the physiologically reasonable parameter values $K_D^{(1)} = 74 \text{ nM}$, $l_{\text{linker}} = 21 \text{ nm}$, $l_{\text{flex}} = 1.8 \text{ nm}$, $\tilde{\alpha} = 5.2 \times 10^5$, and the ssDNA persistence length $\xi_{\text{ssDNA}} = 0.1$. The avidity parameter $\tilde{\alpha}$ is orders of magnitude larger than the corresponding parameter ($\alpha = 70$) in the model neglecting ssDNA because the probability that the 3D random walk encompassed within $\tilde{n}(l_{\text{dsDNA}}, l_{\text{ssDNA}})$ will end at the particular distance to enable bivalent binding is small, thereby requiring a correspondingly larger avidity parameter.

Fig. 2C plots the probability that a diFab will be bivalently bound (p_2) relative to the monovalently bound probability (p_1) as the amount of dsDNA (d) and ssDNA (s) in the linker varies. The model captures the trend that bivalent binding is most likely when $l_{\text{linker}} \approx l_{\text{dsDNA}}$ around $d=62 \text{ bp}$ dsDNA, with the peak shifting very slightly leftwards as the amount of ssDNA increases, demonstrating how the root-mean-squared length of the ssDNA slowly increases. The black curve in Fig. 2D shows how the model incorporating ssDNA (Eq. 9) provides a broader transition of the bivalent to monovalent binding. For the remainder of the paper, we restrict our analysis to this latter model that includes the contributions from both ssDNA and dsDNA within the linker.

The diFab Model Allows Bivalent Binding Only when the dsDNA Length is Approximately Equal to the Length of the Linker it Spans

To gain a qualitative understanding of the model including ssDNA (Eq. 9), we examined it in two limits: near an optimal geometry $l_{\text{dsDNA}} \approx l_{\text{linker}}$ where the ability to bind bivalently is maximum, and far from the optimal limit when the diFab is too short or too long to permit bivalent binding through intra-spike crosslinking. Note that all these statements also hold for the model excluding ssDNA (Eq. 5) provided $\tilde{\alpha} \rightarrow \alpha$ and $\tilde{n} \rightarrow n$.

Near the optimal limit, corresponding to $l_{\text{dsDNA}} \approx l_{\text{linker}}$ or $d \approx 62 \text{ bp}$, HIV-1 neutralization will occur predominantly from the bivalently-bound configuration rather than the monovalent state, $\frac{p_2}{p_1} = \tilde{\alpha} \tilde{n}(l_{\text{dsDNA}}, l_{\text{ssDNA}}) \gg 1$. Hence, the system is well approximated with each spike either being unbound or bivalently-bound such that

$$\text{IC}_{50} \approx \frac{K_D^{(1)}}{\tilde{\alpha} \tilde{n}(l_{\text{dsDNA}}, l_{\text{ssDNA}})}, \quad (\text{near optimal geometry}) \quad \#[\text{Error! Bookmark not defined.}]$$

corresponding to the trough in the black curve in Fig. 2D. If the potency of diFab 1 is $IC_{50}^{(1)}$, and the potency of diFab 2 with a different linker is $IC_{50}^{(2)}$, the latter diFab's potency will be shifted relative to the former by

$$\frac{IC_{50}^{(2)}}{IC_{50}^{(1)}} = \frac{\tilde{n}(l_{dsDNA}^{(1)}, l_{ssDNA}^{(1)})}{\tilde{n}(l_{dsDNA}^{(2)}, l_{ssDNA}^{(2)})} \quad \#[\text{Error! Bookmark not defined.}]$$

In other words, the relative potency of both diFabs is determined solely by the separation distances between the two Fabs in the diFabs, so that the entropy, rather than the energy, determines which diFab will be more effective.

When the linker in a diFab becomes too small ($l_{dsDNA} \lesssim l_{linker} - l_{flex}$) or too large ($l_{dsDNA} \gtrsim l_{linker} + l_{flex}$), the diFab loses the ability to bind bivalently ($n(l_{dsDNA}) \approx 0$) and the IC_{50} attains a constant value

$$IC_{50} \approx K_D^{(1)} \quad (\text{far from optimal geometry}) \quad \#[\text{Error! Bookmark not defined.}]$$

shown as a pink dashed line in Fig. 2D.

Altering the Fraction of ssDNA and dsDNA in the Linker

We next modeled how well the probability of diFab binding (Eq. 9) quantitatively characterized the neutralization of new diFab constructs. We first tuned the rigidity of the linker while keeping the length of the DNA segment fixed. Starting with the optimal construct ($d=62, s=12$), five new diFabs were considered with different amounts of dsDNA d flanked by two ssDNA segments s maintaining $d+2s=86$ bases (Fig. 3A). Fig. 3B shows how the predicted behavior of these constructs using our model.

Extra Long ssDNA Segments are Characterized by a Short Persistence Length

We next modeled diFabs with extra long ssDNA regions to investigate whether the ssDNA in this limit has an appreciable effect (Fig. 4A). If the size of the ssDNA grows slowly with its length, we would expect that constructs with increased ssDNA, such as ($d=62, s=17$) and ($d=62, s=42$), would neutralize less potently than their counterpart ($d=62, s=12$) with the same length of dsDNA.

Adding ssDNA Gaps makes dsDNA Flexible and Decreases diFab Efficacy

As a final probe of the effects of linker flexibility, we investigated the potency of two diFabs in which the dsDNA linker was interspersed with short ssDNA segments (Fig. 5A). These constructs, denoted by $({}_510_510_510_5)$ and $({}_510_522_510_5)$, contained the same lengths of DNA as ($d=50, s=12$) and ($d=62, s=12$). However, the dsDNA in $({}_510_510_510_5)$ and $({}_510_522_510_5)$ was flanked by an extra 5 bases of ssDNA on both sides and interrupted in two places by 5 bases of ssDNA.

Our model can be generalized to analyze these constructs by considering the inner ssDNA segments as simple hinges with no length so that the dsDNA can now be characterized as a random walk composed of three steps (Appendix F). The two outer ssDNA segments can be modeled as a random walk with a persistence length of 0.1 nm. For the larger of the two constructs, $({}_510_522_510_5)$, the 42 bp of dsDNA would account for a maximum of only 14 nm when arranged linearly, thus the two outer ssDNA segments would have to stretch outwards by at least 7 nm (11 bases) to achieve the optimal separation distance of 21 nm in the unlikely event that all of the DNA segments were colinear. The shorter construct in Fig. 5A $({}_510_510_510_5)$ would require the ssDNA to stretch even further to achieve maximal potency. Hence, the two gapped diFabs should only bind monovalently with an IC_{50} given by Eq. 12, as confirmed by the model

in Fig. 5B. Note that even if the dsDNA region of the linker were made longer, increasing the dsDNA flexibility in this manner increases the entropy lost when going from the monovalently- to bivalently-bound states and hence decreases the neutralization potency of the diFab. In Appendix F, we use the model to quantify the decrease in potency as the dsDNA in the optimal ($d=62$, $s=12$) construct is broken into multiple segments.

Discussion

The low density of Env spikes on HIV-1 potentially enables the virus to mitigate the host antibody response by hindering host IgGs from using both antigen-binding Fabs to bind bivalently, thereby expanding the range of HIV-1 mutations permitting antibody evasion (21, 36). The observation that a mutant simian immunodeficiency virus (SIV) with a higher number of Env spikes reverted to its normal spike number of ≈ 14 when propagated in non-human primate hosts is consistent with selection against those viruses that facilitate the ability of host IgGs to bind bivalently through inter-spike crosslinking (54). Although HIV-1 may be more infectious and hence spread more rapidly with more Env trimers (55), the immune system apparently applies selective pressure that keeps the Env spike count per virion low, presumably to prevent anti-HIV-1 IgGs from utilizing avidity effects to counter the lower intrinsic Fab-Env affinities that result from rapid mutation of Env. Antibody isotypes such as dimeric IgA or pentameric IgM have increased valencies (four and ten Fabs, respectively) compared to the two Fabs of an IgG, thus allowing for increased avidity effects during antibody binding to a pathogen. However, most of the neutralizing activity in the sera of HIV-1-positive individuals is attributed to IgGs (56, 57), and converting an anti-HIV-1 IgG broadly neutralizing antibody to an IgA or IgM has minimal effects on potency in standard neutralization assays (58, 59). Thus, most antibodies against HIV-1 Env must resort to monovalent binding by IgGs in the absence of avidity effects that would strengthen their interactions with other pathogens.

Bivalent binding to single Env trimers is another way to utilize avidity effects to counteract the low spike density of HIV-1. Although the architecture of HIV-1 Env trimers prohibits simultaneous binding of both Fabs of conventional, host-derived IgGs (28, 29), we constructed synthetic antibodies (Fig. 1B) (diFabs constructed from Fabs from a neutralizing anti-HIV-1 IgG joined by a linker containing rigid dsDNA flanked by flexible ssDNA) designed to achieve intra-spike crosslinking; i.e., bivalent binding to adjacent Fab binding sites on a single Env trimer. In previous work, we measured the neutralization potencies of an array of diFabs with different dsDNA lengths and found that the linker in the optimal 3BNC60 diFab had 62 bp (21 nm) dsDNA.

The optimal 21 nm length of the dsDNA portion of the linker can be compared to the distance between adjacent 3BNC60 Fabs in various conformations of HIV-1 Envs. It has been shown that HIV-1 Env trimers adopt multiple conformations on virions (23, 60) and in the soluble native-like forms used for structural studies (47). For example, binding of the host CD4 receptor induces outward displacements of the three Env gp120 subunits, resulting in an open conformation in which the coreceptor binding sites on the trimer apex V3 loops are exposed (61-64) and which rearranges further upon coreceptor binding and subsequent membrane fusion. We measured the distances between adjacent 3BNC60 epitopes on Env trimers in different conformations using a new cryo-EM structure of 3BNC117 Fab (a close relative of 3BNC60 (46)) bound to a closed Env trimer (65). Measurements from this single-particle cryo-EM structure allows estimation of the average position of the C-terminal C_H1 domain residue to which the DNA in our diFabs was covalently attached, since Fabs in cryo-EM structures are not influenced by crystal packing forces that can alter the C_H1 - C_L domain position relative to the V_H -

V_L domains in X-ray structures (45). We used the 3BNC117 Fab-gp120 portion of the cryo-EM structure to measure the distance between adjacent Fab C_H1 C-termini in the closed conformation of Env and then modeled a 3BNC60-gp120 protomer into three recent cryo-EM structures of Env trimers in different conformations: an open Env bound by the b12 bNAb in which the coreceptor binding sites on the V3 loops are not exposed (62), an open CD4-bound Env structure with exposed V3 loops (62), and a partially-open CD4-bound Env in which the gp120 subunits adopted positions mid-way between closed and fully open (63). From these structures, we measured distances of 15.8, 20.3, 20.4, and 20.1 nm between C-termini of 3BNC60 Fab C_H1 domains modeled onto the closed, b12-bound open, CD4-bound open, and CD4-bound partially-open Env conformations, respectively (see Methods). Although monovalent CD4-binding site bNAb Fabs bind the closed Env trimer conformation (47), the 21 nm length of the dsDNA in the optimal ($d=62$, $s=12$) diFab more closely matched measured distances for the open Env trimer structures, perhaps indicating that the diFab captured an open Env conformation that could be neutralized potently by a reagent binding through intra-spike crosslinking.

In this work, we consider an array of diFabs with variable amounts of rigid dsDNA and flexible ssDNA, enabling us to tune both the length and rigidity of the DNA linker. In order to provide a conceptual framework to understand how these synthetic antibodies function, we developed a statistical mechanics-based model to predict diFab potencies for inhibiting infection of the 6535.3 strain of HIV-1. By assuming that (i) each homotrimeric spike is unable to help infect a host cell when any one of its three epitopes are bound by Fab, and (ii) that the infectivity of a virion varies linearly with the number of unbound Env, we showed that the neutralization of a virion is proportional to the probability that any single Env protein is bound by a Fab (Appendix A). This framework enabled us to translate the linker-dependent entropy and energy of binding to an HIV-1 Env trimer into a predicted neutralization potency for each diFab.

The first set of diFabs we created explored the effects of linker rigidity. These constructs had the same total length of DNA (86 bases) but differed in their fractions of dsDNA and ssDNA (Fig. 3). We found that as the dsDNA decreased from the optimal $d=62$ to $d=58$, 50, 40, 30, and 20 bp, the potency of the antibodies rapidly decreased so that the four constructs with $d \leq 50$ neutralized only as effectively as the monovalent Fab. From a modeling perspective, the short ssDNA persistence length implies that the ssDNA plays a minor role in determining diFab potency. Hence, the constructs composed of d bp dsDNA and $s=(86-d)/2$ bases ssDNA should behave similarly to the constructs with d bp dsDNA and $s=12$ bases ssDNA. In other words, decreasing the dsDNA length shortened the length of the diFabs to the point where only monovalent binding was possible when $d \leq 50$. A second set of diFabs explored whether extra long ssDNA segments can alter diFab potency (Fig. 4). The observed effects were minor, reaffirming that the length of dsDNA in the linker has greater impact on diFab potency than the length of ssDNA. Finally, we considered two additional diFabs that introduced ssDNA gaps within the dsDNA portion of the linker (Fig. 5). As in the above two cases, the model predicts that both constructs should exhibit poor neutralization potencies comparable to that of a monovalent Fab (see Appendix F).

We point out several factors of the HIV-1 system that the model neglects. First, the model does not consider potential diFab binding between adjacent Env trimers, although this binding should be minimal given the low density of Env on the virion's surface. Second, our model assumed that the % neutralization of HIV-1 decreases linearly with the number of unbound Env trimers (Appendix A); such a linear relationship has been observed when less than half the HIV-1 spikes are bound (55), although it may not hold when more than half of the spikes are bound

(possibly because some minimum number of unbound Env trimers are needed to successfully infect a cell). In a similar vein, we neglected the variability in the numbers of spikes per virion (22-25), instead assuming that all virions had exactly 14 spikes. However, relaxing these assumptions yielded nearly identical results (Appendix A), suggesting that the model is robust to these assumptions.

A compelling extension of this work that would deepen our understanding of the antibody response against HIV-1 would be to consider reagents with more than two Fabs. As has been seen in other biological systems (66-68), synthetic antibodies with greater valency can elicit tighter binding. Hence, a triFab that allows three Fabs to simultaneously bind to an HIV-1 Env trimer is predicted to have a lower IC_{50} than an optimal diFab; indeed, our model predicts that an optimal triFab would have an IC_{50} that is 100x more potent than the optimal ($d=62$, $s=12$) diFab (see Appendix F). Modeling verifies that a rigid linker is required for a bivalent or trivalent reagent to achieve avidity effects by intra-spike crosslinking, thus providing guidance for constructing optimal anti-HIV-1 therapeutics that remain potent against HIV-1 in the face of the Env mutations arising during HIV-1 replication.

Multivalency has been harnessed in an array of fields that extend beyond immunology; e.g., novel materials and scaffolds have been designed at the super-cellular scale using multivalency (69), and molecular targeting and molecular machines employ multivalency at the molecular scale (68, 70, 71). We hope that our work presents a step towards precise, quantitative models that encompasses multivalent binding in each of these contexts.

Methods

Measurements of Separation Distances on Env Trimer Structures

We used a single-particle cryo-EM structure (65) of a closed Env trimer bound to 3BNC117, a 3BNC60-related bNAb (46) for estimating the position of position of C_{H1} residue 233 (to which the DNA linker in the 3BNC60 diFabs was attached) when a 3BNC60 diFab is bound to an Env trimer. The coordinates for the V_H-V_L domains of the 3BNC60 Fab (46) were superimposed on the 3BNC117 V_H-V_L domains, and the coordinates for the C_{H1}-C_L domains from the structure of b12 IgG (27) were superimposed on the 3BNC117 C_{H1}-C_L domains because C_{H1} residues 217 – 233 are disordered in the 3BNC60 Fab structure (46). The model for the 3BNC60 Fab-gp120 portion of the trimeric cryo-EM complex structure was used to measure the distance between adjacent Fab C_{H1} C-termini in the closed conformation of Env and then modeled into three cryo-EM structures of Envs in different conformations: an open Env bound by the b12 bNAb in which the coreceptor binding sites on the V3 loops are not exposed (62), an open CD4-bound Env structure with exposed V3 loops (62), and a partially-open CD4-bound Env in which the gp120 subunits adopted positions mid-way between closed and fully open (63).

Author Contributions

T.E., P.J.B., and R.P. conceived the project and interpreted results; T.E., S.Y., and R.P. developed the model and performed analyses; T.E., R.P., and P.J.B. wrote the paper with input from other authors.

Acknowledgements

We thank Anthony Bartolotta, Justin Bois, Jim Eisenstein, Vahe Galstyan, Peng He, Willem Hegel, David Hsieh, Giacomo Koszegi, Pankaj Mehta, Jiseon Min, Olexei Motrunich, Noah Olsman, Vahe Singh, and Richard Zhu for useful discussions, Christopher Barnes for measuring modeled 3BNC60-Env complexes, Aaron Coey for discussions about triFabs IC₅₀s, and affinities, and Marta Murphy for help with preparing figures. This research was supported by National Institute of Allergy and Infectious Diseases of the National Institutes of Health grants 1R01AI129784 and HIVRAD P01 AI100148 (P.J.B.), the Bill and Melinda Gates Foundation Collaboration for AIDS Vaccine Discovery Grant 1040753 (P.J.B.), La Fondation Pierre-Gilles de Gennes (R.P.), the Rosen Center at Caltech (R.P.), the National Institutes of Health DP1 OD000217 (Director's Pioneer Award), R01 GM085286, and 1R35 GM118043-01 (MIRA) (R.P.), and a Caltech-COH Biomedical Research Initiative (to P.J.B.). We are grateful to the Burroughs-Wellcome Fund for its support of the Physiology Course at the Marine Biological Laboratory, where part of the work on this work was done, and for a post-course research grant (S.Y.).

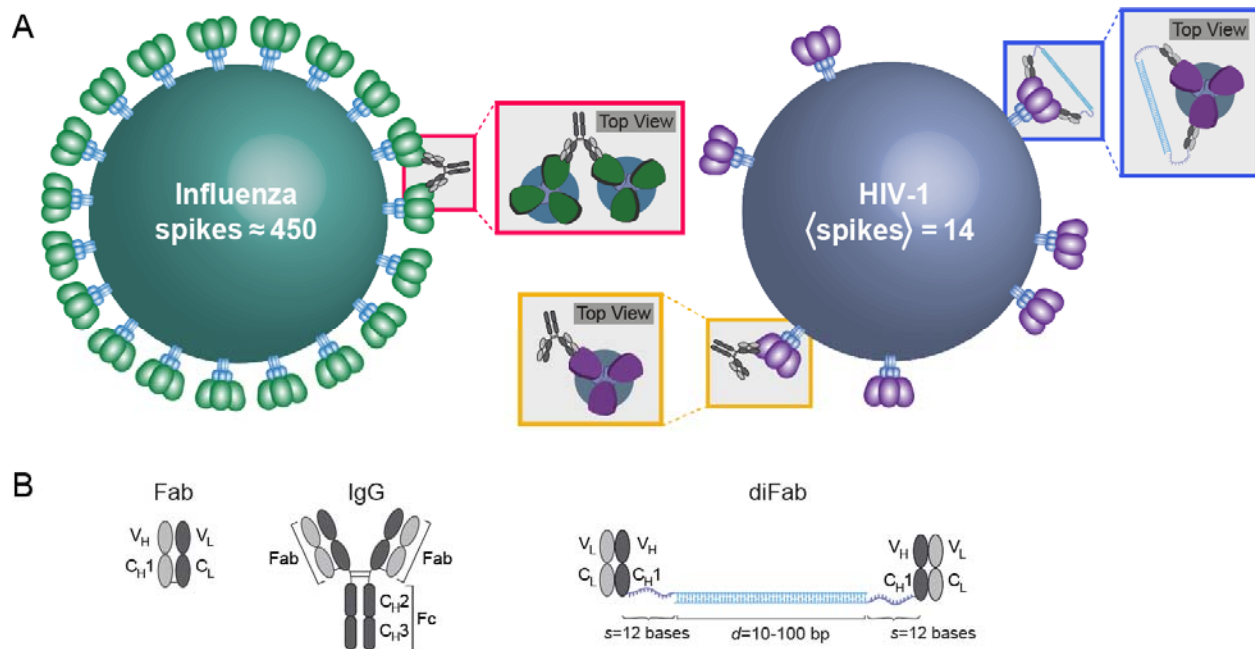


Fig. 1. Effects of spike density on IgG binding. (A) Close spacing of hundreds of surface spikes on influenza A allows bivalent binding of IgGs to adjacent spikes (red boxes), permitting avidity effects in the context of low monovalent (i.e., Fab-antigen) affinities. In contrast, HIV-1 has an average of 14 spikes that are spaced far apart, and because the HIV-1 spike architecture prohibits simultaneous binding of two Fabs to a single Env trimer, most IgGs bind monovalently to HIV-1 Envs (gold boxes). We investigated a synthetic homo-diFab designed to bind bivalently to a single HIV-1 spike trimer (blue boxes). (B) Schematics of a Fab, an IgG, and a diFab composed of two Fabs joined by a ssDNA and dsDNA linker of length d bp flanked on both sides by $s=12$ bases of ssDNA.

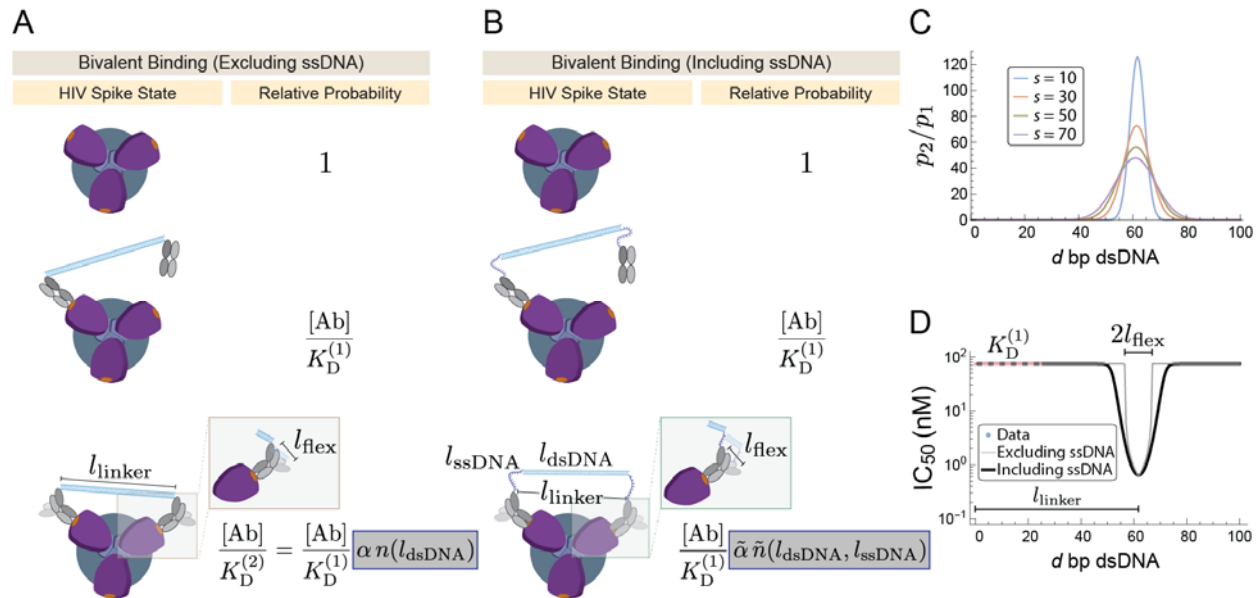


Fig. 2. Modeling the optimal linker length for a diFab. (A) DLS data suggested that the diFab linker can be modeled by either (A) ignoring the ssDNA entirely or (B) including the ssDNA with a smaller persistence length. In both models, the Boltzmann weight of the monovalent state is dictated by the $K_D^{(1)}$ (the dissociation constant between the Env trimer and the first diFab arm), while the weight of the bivalent state is dictated by a geometric or avidity factor (αn in Panel A and $\tilde{\alpha} \tilde{n}$ in Panel B) shown in a gray box. This geometric factor depends upon the length of the dsDNA and ssDNA in each construct as well as on the optimal length l_{linker} of the linker between two bound Fabs and the flexibility l_{flex} between the C_H1-C_L and V_H-V_L domains of a bound Fab. The ability to neutralize is given by the sum of the probabilities of the monovalent and bivalent states. (C) The relative probability that a diFab with d bp dsDNA and s bases ssDNA in its linker is bivalently (p_2) versus monovalently (p_1) bound. (D) Predicted effects of dsDNA bridge lengths on the neutralization potencies of the 3BNC60 diFabs against HIV-1 strain 6535.3.

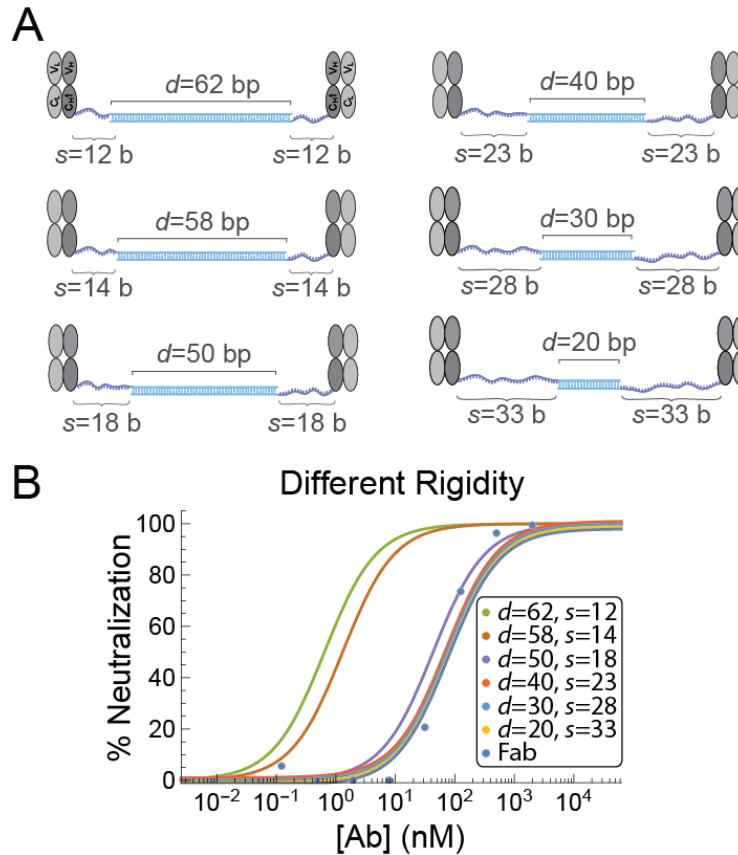


Fig. 3. Effects of linker rigidity on diFab potency. (A) Schematics of 3BNC60 diFabs with different proportions of dsDNA and ssDNA in their linkers. The linkers were constructed to span 86 bases of DNA, of which $d = 62, 58, 50, 40, 30,$ or 20 bases were dsDNA. (B) Model predictions for the neutralization potency of these constructs. Data points show a representative in vitro neutralization assay of the 3BNC60 Fab against HIV-1 strain 6535.3 ($n = 13$ replicates).

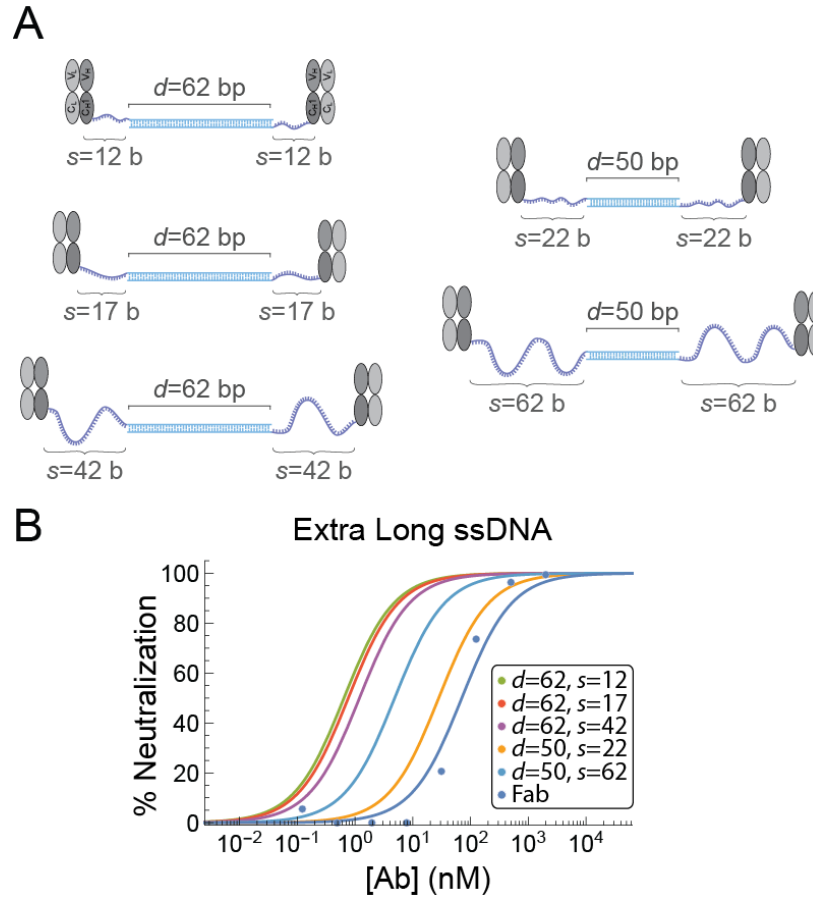


Fig. 4. Effects of extra long ssDNA in linkers on diFab potency. (A) Schematics of 3BNC60 diFabs. (B) Model predictions for the neutralization potency of these constructs. Data points show a representative in vitro neutralization assay of the 3BNC60 Fab against HIV-1 strain 6535.3 ($n = 13$ replicates).

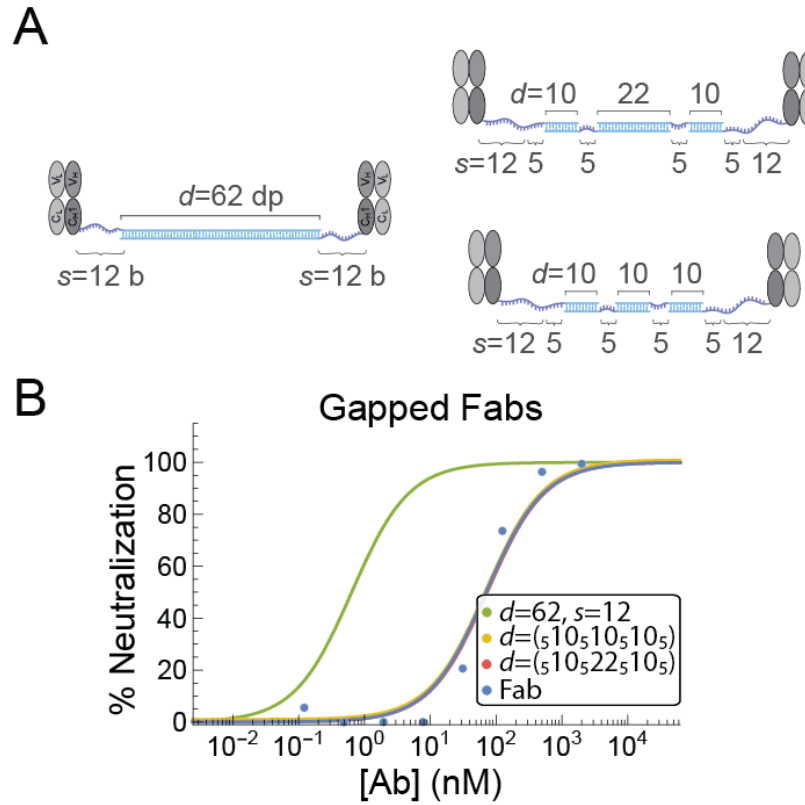


Fig. 5. Effects of gaps in dsDNA portions of diFab linkers on potency. (A) Schematics of 3BNC60 diFabs with ssDNA gaps interspersed within the dsDNA portion of the linker. (B) Model predictions for the neutralization potency of these constructs. Data points show a representative in vitro neutralization assay of the 3BNC60 Fab against HIV-1 strain 6535.3 ($n = 13$ replicates).

References

1. UNAIDS (2017) UNAIDS Data 2017.
2. Fauci AS (2008) 25 years of HIV. *Nature* 453(7193):289-90.
3. Escolano A, Dosenovic P, Nussenzweig MC (2017) Progress toward active or passive HIV-1 vaccination. *J Exp Med* 214(1):3-16.
4. McCoy LE, Burton DR (2017) Identification and specificity of broadly neutralizing antibodies against HIV. *Immunol Rev* 275(1):11-20.
5. Klasse PJ (2012) The molecular basis of HIV entry. *Cell Microbiol* 14(8):1183-92.
6. Baba TW, Liska V, Hofmann-Lehmann R, Vlasak J, Xu W, Ayehunie S, et al. (2000) Human neutralizing monoclonal antibodies of the IgG1 subtype protect against mucosal simian-human immunodeficiency virus infection. *Nat Med* 6(2):200-6.
7. Mascola JR, Stiegler G, VanCott TC, Katinger H, Carpenter CB, Hanson CE, et al. (2000) Protection of macaques against vaginal transmission of a pathogenic HIV-1/SIV chimeric virus by passive infusion of neutralizing antibodies. *Nat Med* 6(2):207-10.
8. Hessel AJ, Rakasz EG, Poignard P, Hangartner L, Landucci G, Forthal DN, et al. (2009) Broadly neutralizing human anti-HIV antibody 2G12 is effective in protection against mucosal SHIV challenge even at low serum neutralizing titers. *PLoS Pathog* 5(5):e1000433.
9. Hessel AJ, Hangartner L, Hunter M, Havenith CE, Beurskens FJ, Bakker JM, et al. (2007) Fc receptor but not complement binding is important in antibody protection against HIV. *Nature* 449(7158):101-4.
10. Klein F, Halper-Stromberg A, Horwitz JA, Gruell H, Scheid JF, Bournazos S, et al. (2012) HIV therapy by a combination of broadly neutralizing antibodies in humanized mice. *Nature* 492(7427):118-22.
11. Klein F, Mouquet H, Dosenovic P, Scheid JF, Scharf L, Nussenzweig MC (2013) Antibodies in HIV-1 vaccine development and therapy. *Science* 341(6151):1199-204.
12. Klein F, Nogueira L, Nishimura Y, Phad G, West AP, Jr., Halper-Stromberg A, et al. (2014) Enhanced HIV-1 immunotherapy by commonly arising antibodies that target virus escape variants. *J Exp Med* 211(12):2361-72.
13. Caskey M, Klein F, Lorenzi JC, Seaman MS, West AP, Jr., Buckley N, et al. (2015) Viraemia suppressed in HIV-1-infected humans by broadly neutralizing antibody 3BNC117. *Nature* 522(7557):487-91.
14. Caskey M, Schoofs T, Gruell H, Settler A, Karagounis T, Kreider EF, et al. (2017) Antibody 10-1074 suppresses viremia in HIV-1-infected individuals. *Nat Med* 23(2):185-91.
15. Lynch RM, Boritz E, Coates EE, DeZure A, Madden P, Costner P, et al. (2015) Virologic effects of broadly neutralizing antibody VRC01 administration during chronic HIV-1 infection. *Science translational medicine* 7(319):319ra206.
16. Schoofs T, Klein F, Braunschweig M, Kreider EF, Feldmann A, Nogueira L, et al. (2016) HIV-1 Immunotherapy with Monoclonal Antibody 3BNC117 Elicits Host Immune Responses against HIV-1. *Science* 352(6288):997-1001.
17. Moore PL, Gray ES, Wibmer CK, Bhiman JN, Nonyane M, Sheward DJ, et al. (2012) Evolution of an HIV glycan-dependent broadly neutralizing antibody epitope through immune escape. *Nat Med* 18(11):1688-92.
18. Liao HX, Lynch R, Zhou T, Gao F, Alam SM, Boyd SD, et al. (2013) Co-evolution of a broadly neutralizing HIV-1 antibody and founder virus. *Nature* 496(7446):469-76.
19. Wibmer CK, Bhiman JN, Gray ES, Tumba N, Abdool Karim SS, Williamson C, et al. (2013) Viral escape from HIV-1 neutralizing antibodies drives increased plasma neutralization breadth through sequential recognition of multiple epitopes and immunotypes. *PLoS Pathog* 9(10):e1003738.

20. Doria-Rose NA, Schramm CA, Gorman J, Moore PL, Bhiman JN, DeKosky BJ, et al. (2014) Developmental pathway for potent V1V2-directed HIV-neutralizing antibodies. *Nature* 509(7498):55-62.
21. Klein JS, Bjorkman PJ (2010) Few and far between: how HIV may be evading antibody avidity. *PLoS Pathog* 6(5):e1000908.
22. Chertova E, Bess Jr JW, Jr., Crise BJ, Sowder IR, Schaden TM, Hilburn JM, et al. (2002) Envelope glycoprotein incorporation, not shedding of surface envelope glycoprotein (gp120/SU), is the primary determinant of SU content of purified human immunodeficiency virus type 1 and simian immunodeficiency virus. *J Virol* 76(11):5315-25.
23. Liu J, Bartesaghi A, Borgnia MJ, Sapiro G, Subramaniam S (2008) Molecular architecture of native HIV-1 gp120 trimers. *Nature* 455(7209):109-13.
24. Zhu P, Chertova E, Bess J, Jr., Lifson JD, Arthur LO, Liu J, et al. (2003) Electron tomography analysis of envelope glycoprotein trimers on HIV and simian immunodeficiency virus virions. *Proc Natl Acad Sci USA* 100(26):15812-7.
25. Zhu P, Liu J, Bess J, Jr., Chertova E, Lifson JD, Grise H, et al. (2006) Distribution and three-dimensional structure of AIDS virus envelope spikes. *Nature* 441(7095):847-52.
26. Patel P, Borkowf CB, Brooks JT, Lasry A, Lansky A, Mermin J (2014) Estimating per-act HIV transmission risk: a systematic review. *AIDS (London, England)* 28(10):1509-19.
27. Saphire EO, Parren PW, Pantophlet R, Zwick MB, Morris GM, Rudd PM, et al. (2001) Crystal structure of a neutralizing human IgG against HIV-1: a template for vaccine design. *Science* 293(5532):1155-9.
28. Klein JS (2009) Investigations in the design and characterization of HIV-1 neutralizing molecules. Pasadena: California Institute of Technology.
29. Wang H, Gristick HB, Scharf L, West AP, Galimidi RP, Seaman MS, et al. (2017) Asymmetric recognition of HIV-1 Envelope trimer by V1V2 loop-targeting antibodies. *Elife* 6.
30. Layne SP, Merges MJ, Dembo M, Spouge JL, Conley SR, Moore JP, et al. (1992) Factors underlying spontaneous inactivation and susceptibility to neutralization of human immunodeficiency virus. *Virology* 189(2):695-714.
31. Eisen HN, Siskind GW (1964) Variations in Affinities of Antibodies during the Immune Response. *Biochemistry* 3:996-1008.
32. Azimzadeh A, Van Regenmortel MH (1990) Antibody affinity measurements. *J Mol Recognit* 3(3):108-16.
33. Kiessling LL, Lamanna AC (2003) Multivalency in Biological Systems. In: Schneider MP, editor. *Chemical Probes in Biology NATO Science Series (Series II: Mathematics, Physics and Chemistry)*. 129: Springer, Dordrecht.
34. Krishnamurthy VM, Estroff LA, Whitesides GM (2006) *Multivalency in Ligand Design*: Wiley - VCH Verlag GmbH & Co. KGaA.
35. Karush F (1976) Multivalent binding and functional affinity. *Contemp Top Mol Immunol* 5:217-28.
36. Galimidi RP, Klein JS, Politzer MS, Bai S, Seaman MS, Nussenzweig MC, et al. (2015) Intra-spike crosslinking overcomes antibody evasion by HIV-1. *Cell* 160(3):433-46.
37. Bednar J, Furrer P, Katritch V, Stasiak AZ, Dubochet J, Stasiak A (1995) Determination of DNA persistence length by cryo-electron microscopy. Separation of the static and dynamic contributions to the apparent persistence length of DNA. *J Mol Biol* 254(4):579-94.
38. Klein JS, Jiang S, Galimidi RP, Keeffe JR, Bjorkman PJ (2014) Design and characterization of structured protein linkers with differing flexibilities. *Protein Engineering, Design, and Selection* 27:325-30.
39. Montefiori DC (2005) Evaluating neutralizing antibodies against HIV, SIV, and SHIV in luciferase reporter gene assays. *Current protocols in immunology* / edited by John E Coligan [et al Chapter 12:Unit 12 1.

40. Merk A, Subramaniam S (2013) HIV-1 envelope glycoprotein structure. *Curr Opin Struct Biol* 23(2):268-76.
41. Brunet A, Tardin C, Salomé L, Rousseau P, Destainville N, Manghi M (2015) Dependence of DNA Persistence Length on Ionic Strength of Solutions with Monovalent and Divalent Salts: A Joint Theory–Experiment Study. *Macromolecules* 48(11):3641-52.
42. Ambia-Garrido J, Vainrub A, Pettitt BM (2010) A model for Structure and Thermodynamics of ssDNA and dsDNA Near a Surface: a Coarse Grained Approach. *Comput Phys Commun* 181(12):2001-7.
43. Tinland B, Pluen A, Sturm J, Weill G (1997) Persistence Length of Single-Stranded DNA. *Macromolecules* 30(19):5763–5.
44. Doi M, Edwards SF (1986) Static Properties of Polymers. *The Theory of Polymer Dynamics*. Oxford, UK: Oxford University Press.
45. Stanfield RL, Zemla A, Wilson IA, Rupp B (2006) Antibody elbow angles are influenced by their light chain class. *J Mol Biol* 357(5):1566-74.
46. Scheid JF, Mouquet H, Ueberheide B, Diskin R, Klein F, Olivera TY, et al. (2011) Sequence and Structural Convergence of Broad and Potent HIV Antibodies That Mimic CD4 Binding. *Science* 333:1633-7.
47. Ward AB, Wilson IA (2017) The HIV-1 envelope glycoprotein structure: nailing down a moving target. *Immunol Rev* 275(1):21-32.
48. Brandenberg OF, Magnus C, Rusert P, Gunthard HF, Regoes RR, Trkola A (2017) Predicting HIV-1 transmission and antibody neutralization efficacy in vivo from stoichiometric parameters. *PLoS Pathog* 13(5):e1006313.
49. Brandenberg OF, Magnus C, Rusert P, Regoes RR, Trkola A (2015) Different infectivity of HIV-1 strains is linked to number of envelope trimers required for entry. *PLoS Pathog* 11(1):e1004595.
50. Klasse PJ (2007) Modeling how many envelope glycoprotein trimers per virion participate in human immunodeficiency virus infectivity and its neutralization by antibody. *Virology* 369(2):245-62.
51. Yang X, Kurteva S, Ren X, Lee S, Sodroski J (2005) Stoichiometry of envelope glycoprotein trimers in the entry of human immunodeficiency virus type 1. *J Virol* 79(19):12132-47.
52. Phillips R, Kondev J, Theriot J, Garcia HG (2013) *Physical Biology of the Cell*. Second ed. London and New York: Garland Science (Taylor & Francis Group).
53. Lyumkis D, Julien JP, de Val N, Cupo A, Potter CS, Klasse PJ, et al. (2013) Cryo-EM structure of a fully glycosylated soluble cleaved HIV-1 envelope trimer. *Science* 342(6165):1484-90.
54. Zingler K, Littman DR (1993) Truncation of the cytoplasmic domain of the simian immunodeficiency virus envelope glycoprotein increases env incorporation into particles and fusogenicity and infectivity. *J Virol* 67(5):2824-31.
55. Layne SP, Merges MJ, Dembo M, Spouge JL, Nara PL (1990) HIV requires multiple gp120 molecules for CD4-mediated infection. *Nature* 346(6281):277-9.
56. Scheid JF, Mouquet H, Feldhahn N, Seaman MS, Velinzon K, Pietzsch J, et al. (2009) Broad diversity of neutralizing antibodies isolated from memory B cells in HIV-infected individuals. *Nature* 458(7238):636-40.
57. Tomaras GD, Yates NL, Liu P, Qin L, Fouda GG, Chavez LL, et al. (2008) Initial B-cell responses to transmitted human immunodeficiency virus type 1: virion-binding immunoglobulin M (IgM) and IgG antibodies followed by plasma anti-gp41 antibodies with ineffective control of initial viremia. *J Virol* 82(24):12449-63.
58. Kunert R, Wolbank S, Stiegler G, Weik R, Katinger H (2004) Characterization of molecular features, antigen-binding, and in vitro properties of IgG and IgM variants of 4E10, an anti-HIV type 1 neutralizing monoclonal antibody. *AIDS Res Hum Retroviruses* 20(7):755-62.

59. Wolbank S, Kunert R, Stiegler G, Katinger H (2003) Characterization of human class-switched polymeric (immunoglobulin M [IgM] and IgA) anti-human immunodeficiency virus type 1 antibodies 2F5 and 2G12. *J Virol* 77(7):4095-103.
60. Munro JB, Gorman J, Ma X, Zhou Z, Arthos J, Burton DR, et al. (2014) Conformational dynamics of single HIV-1 envelope trimers on the surface of native virions. *Science* 346(6210):759-63.
61. Harris A, Borgnia MJ, Shi D, Bartesaghi A, He H, Pejchal R, et al. (2011) Trimeric HIV-1 glycoprotein gp140 immunogens and native HIV-1 envelope glycoproteins display the same closed and open quaternary molecular architectures. *Proc Natl Acad Sci U S A* 108(28):11440-5.
62. Ozorowski G, Pallesen J, de Val N, Lyumkis D, Cottrell CA, Torres JL, et al. (2017) Open and closed structures reveal allostery and pliability in the HIV-1 envelope spike. *Nature* 547(7663):360-3.
63. Wang H, Barnes CO, Yang Z, Nussenzweig MC, Bjorkman PJ (2018) Partially-open HIV-1 Envelope Exhibit Conformational Changes Relevant for Coreceptor Binding and Fusion. *Cell Host Microbe*:in press.
64. Wang H, Cohen AA, Galimidi RP, Gristick HB, Jensen GJ, Bjorkman PJ (2016) Cryo-EM structure of a CD4-bound open HIV-1 envelope trimer reveals structural rearrangements of the gp120 V1V2 loop. *Proc Natl Acad Sci U S A* 113(46):E7151-E8.
65. Lee JH, Andrabi R, Su CY, Yasmeen A, Julien JP, Kong L, et al. (2017) A Broadly Neutralizing Antibody Targets the Dynamic HIV Envelope Trimer Apex via a Long, Rigidified, and Anionic beta-Hairpin Structure. *Immunity* 46(4):690-702.
66. Kitov PI, Bundle DR (2003) On the nature of the multivalency effect: a thermodynamic model. *J Am Chem Soc* 125(52):16271-84.
67. Liese S, Netz RR (2015) Influence of length and flexibility of spacers on the binding affinity of divalent ligands. *Beilstein J Org Chem* 11:804-16.
68. Yan GH, Wang K, Shao Z, Luo L, Song ZM, Chen J, et al. (2018) Artificial antibody created by conformational reconstruction of the complementary-determining region on gold nanoparticles. *Proc Natl Acad Sci U S A* 115(1):E34-E43.
69. Fasting C, Schalley CA, Weber M, Seitz O, Hecht S, Kokschi B, et al. (2012) Multivalency as a chemical organization and action principle. *Angew Chem Int Ed Engl* 51(42):10472-98.
70. Thubagere AJ, Li W, Johnson RF, Chen Z, Doroudi S, Lee YL, et al. (2017) A cargo-sorting DNA robot. *Science* 357(6356).
71. Varner CT, Rosen T, Martin JT, Kane RS (2015) Recent advances in engineering polyvalent biological interactions. *Biomacromolecules* 16(1):43-55.